HHS Public Access

Author manuscript

Nano Lett. Author manuscript; available in PMC 2015 December 10.

Published in final edited form as:

Nano Lett. 2014 December 10; 14(12): 6792–6798. doi:10.1021/nl5027953.

Sample-Averaged Biexciton Quantum Yield Measured by Solution-Phase Photon Correlation

Andrew P. Beyler, **Thomas S. Bischof**, **Jian Cui**, **Igor Coropceanu**, **Daniel K. Harris**, and **Moungi G. Bawendi***

Department of Chemistry, Massachusetts Institute of Technology, Cambridge, Massachusetts 02139, United States

Abstract

The brightness of nanoscale optical materials such as semiconductor nanocrystals is currently limited in high excitation flux applications by inefficient multiexciton fluorescence. We have devised a solution-phase photon correlation measurement that can conveniently and reliably measure the average biexciton-to-exciton quantum yield ratio of an entire sample without user selection bias. This technique can be used to investigate the multiexciton recombination dynamics of a broad scope of synthetically underdeveloped materials, including those with low exciton quantum yields and poor fluorescence stability. Here, we have applied this method to measure weak biexciton fluorescence in samples of visible-emitting InP/ZnS and InAs/ZnS core/shell nanocrystals, and to demonstrate that a rapid CdS shell growth procedure can markedly increase the biexciton fluorescence of CdSe nanocrystals.

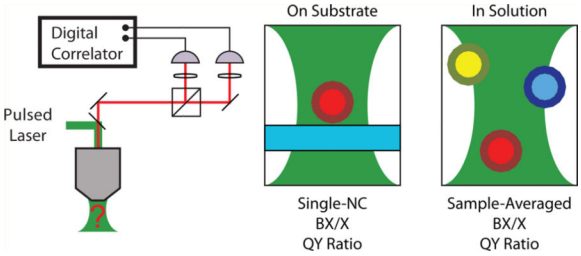

Keywords

Photon correlation; single-molecule spectroscopy; semiconductor nanocrystals; multiexcitons

The performance of optical materials in high excitation flux optical applications, such as solid state lighting and confocal biological imaging, is determined by a unique set of optical properties. For example, whereas brightness under low-flux excitation is determined by the

***Corresponding Author**. mgb@mit.edu.

ASSOCIATED CONTENT

s Supporting Information

A derivation of eqs 2–4, a discussion of several common artifacts and aberrations of the S-$g^{(2)}$ experiment, and the synthetic details of the NC samples studied in this Letter. This material is available free of charge via the Internet at http://pubs.acs.org.

The authors declare no competing financial interest.

product of quantum yield and absorption cross section, fluorescence output in the high-flux regime is primarily limited by the radiative lifetime because each emitter is in a state of perpetual excitation.[1] Single-photon emitters with long radiative lifetimes will reach saturation at much lower excitation fluxes and produce fewer total photons compared to alternatives with short radiative lifetimes. However, for emitters capable of sustaining multiple excitations simultaneously, multiexciton fluorescence provides a means for overcoming fluorescence saturation and enabling higher fluorescence output under high-flux excitation.

Semiconductor nanocrystals (NCs) are a key example of a system whose high-flux suitability is reliant on multiexciton fluorescence. Recent advances in the synthesis of colloidal NCs have improved their quantum yields, size monodispersity, fluorescence stability, compactness, and spectral tunability.[2–4] These innovations have made NCs attractive candidates for many applications throughout the visible, short-wave infrared, and mid-infrared optical regions spanning 400–5000 nm.[5–8] Nevertheless, they are not currently well-optimized for high-flux applications because of their relatively long radiative lifetimes, ranging from tens of nanoseconds for CdSe samples to hundreds of nanoseconds or microseconds for infrared-emitting PbS and PbSe samples,[9–11] and because of their low multiexciton quantum yields, caused by efficient Auger-like and other nonradiative recombination pathways.[12–14] Our poor understanding and control of these competing multiexcitonic processes has been a limiting factor in the development of NCs for high-flux optical applications.

Multiexciton recombination dynamics have conventionally been studied using two distinct approaches. On one hand, ultrafast techniques such as transient absorption and transient photoluminescence can be used to measure the lifetime of multiexcitons compared to that of single excitons.[13,15–17] These experiments effectively characterize the average properties of entire samples, but rely on the careful modeling of multi-exponential decay curves, are prone to charging artifacts,[18] and require ultrafast capabilities. On the other hand, single-molecule photon-correlation experiments (SM-$g^{(2)}$) can be used to directly assess the effects of competing nonradiative pathways at the single-molecule level by measuring the ratio of the biexciton (BX) and excition (X) fluorescence quantum yields.[19] This technique measures the observable most pertinent for applications without the need for modeling, but cannot always be used to characterize the average properties of entire samples. Nanocrystal samples, for instance, are known to exhibit wide BX quantum yield heterogeneity,[14,20,21] which makes extrapolating the average behavior of a sample from single-NC measurements both time-consuming and prone to selection bias. A convenient and reliable technique for gauging the average multiexciton quantum yields of ensembles would greatly assist in the synthetic effort to improve the efficiency of multiexciton fluorescence.

In this Letter, we demonstrate that the photon-correlation scheme used to measure the BX/X quantum yield ratio of single emitters can be ensemble-averaged over an entire sample by analyzing a dilute solution of emitters instead of a single molecule. This solution-phase experiment (S-$g^{(2)}$) combines many of the advantages of its single-molecule analogue with the advantages of solution-phase measurements, including non-perturbative experimental conditions, ensemble-level statistics, high signal-to-noise ratios, and the lack of user

selection bias. We illustrate the wide applicability of this technique using NCs by examining several synthetically underdeveloped materials and by assessing the BX fluorescence properties produced by our recent rapid CdS shell growth.[22]

Photon correlation is a common analysis technique for studying intensity fluctuations in low-signal samples such as single molecules and dilute solutions.[23] The experimental apparatus for this class of experiments is typified by our setup, shown in Figure 1a. A sample is excited in an epifluorescence microscope, and the resulting emission is collected, split into two channels in a Hanbury Brown and Twiss geometry,[24] and detected by two avalanche photodiodes operating in a single-photon-counting Geiger mode. Then, the two discrete signals are cross-correlated by histogramming the arrivals of pairs of photons according to their temporal separation τ and normalizing based on the overall intensities of both channels according to eq 1.

$$g^{(2)}_{\mathrm{a,b}}(\tau)=\frac{\langle I_{\mathrm{a}}(t)I_{\mathrm{b}}(t+\tau)\rangle}{\langle I_{\mathrm{a}}(t)\rangle\langle I_{\mathrm{b}}(t+\tau)\rangle} \quad (1)$$

Here, $I_{\mathrm{a}}(t)$ and $I_{\mathrm{b}}(t)$ are the intensities on each of the two detectors and $\langle\cdots\rangle$ denotes a time average over the integration time of the experiment. Because there is no bias in the splitting of the signal between detection channels, $g^{(2)}_{\mathrm{a,b}}(\tau)$ is taken to represent the intensity autocorrelation of the total signal, $g^{(2)}(\tau)$. The intensity autocorrelation is directly proportional to the conditional probability of detecting a photon from the sample, given that a photon was already detected some time τ before. A value of unity is consistent with a random, uncorrelated stream of photon arrivals dictated by Poisson statistics. In contrast, a nonunity value reflects correlated structure in the fluorescence intensity of the sample, which may be tied to a variety of physical phenomena or experimental conditions.

Nair et al.[19] pioneered the use of the SM-$g^{(2)}$ photon correlation experiment for studying the multiexciton recombination dynamics of single molecules. In SM-$g^{(2)}$, an individual emitter is excited by a pulsed laser with a pulse duration much shorter than the emitter's fluorescence lifetime and a repetition period much longer than its fluorescence lifetime. Under these conditions, the measured $g^{(2)}(\tau)$ is composed of a series of regularly spaced peaks separated by the repetition period of the laser because fluorescence events preferentially occur following excitation pulses. If the studied fluorophore is a true single-photon emitter, there will not be a "center peak" at $\tau = 0$ because the single molecule cannot emit more than one photon following a single excitation pulse.[25,26] However, Nair et al. showed that single NCs capable of multiexciton fluorescence do exhibit a measurable center peak in their $g^{(2)}(\tau)$. They demonstrated that, under low-flux excitation with photons of energy well above the NC band gap, the ratio of $g^{(2)}_0$, the area of the center peak, to $g^{(2)}_{T_{\mathrm{rep}}}$, the area of the first "side peak" centered at the repetition period of the laser, informs on the relationship between the BX quantum yield and the X quantum yield. That is,

$$\frac{g^{(2)}_0}{g^{(2)}_{T_{\mathrm{rep}}}}=\frac{\langle\gamma_{\mathrm{x}}\gamma_{\mathrm{bx}}\rangle}{\langle\gamma_{\mathrm{x}}^2\rangle} \quad (2)$$

where γ_{bx} is the quantum yield of biexciton fluorescence and γ_x is the quantum yield of exciton fluorescence. The right side of eq 2 is the ratio of the intensity-weighted averages of the BX and X quantum yields of the single NC. In the event of fluorescence intensity fluctuations, these weighted averages preferentially report on their respective quantum yields during periods of high fluorescence intensity because that is when correlation counts are most readily produced. The derivation of this expression hinges on the idea that because the exciton and biexciton have the same absorption cross sections under above-band gap excitation, there is an equal probability of either creating a biexciton in a single excitation pulse or creating two excitons in subsequent excitation pulses. As a result, any reduction in the area of the center peak compared to the area of the side peak is caused by a reduction of the biexciton quantum yield compared to the exciton quantum yield.

Our strategy is to sample-average the SM-$g^{(2)}$ measurement by combining it with fluorescence correlation spectroscopy (FCS). In FCS, the correlation function is measured for a small focal volume of freely diffusing fluorophores in solution that is illuminated by continuous-wave excitation. Because the diffusion of individual particles into and out of the focal volume produces short bursts of fluorescence intensity, the overall signal from the focal volume exhibits photon bunching in its $g^{(2)}(\tau)$, which can be analyzed to reveal diffusion physics.[27] The magnitude of this enhanced correlation at short τ is inversely proportional to the average number of particles in the focal volume, which informs on particle concentration, and the time scale of its decay to unity at long τ is given by their average dwell time in the focal volume, which informs on the hydrodynamic radii of the particles.

As in the SM-$g^{(2)}$ experiment, FCS also reveals photon antibunching at very short τ, on the order of the fluorescence lifetime of the emitters.[28] However, its manifestation in solution exhibits two key differences. First, FCS necessarily informs on the properties of the sample as a whole because of the free and rapid exchange of particles in the focal volume. On the basis of the typical diffusion times of organic dyes and NCs,[29] millions of particles will travel through the focal volume and contribute to the total correlation signal measured over the course of an hour long experiment. And second, the antibunching feature of single-photon emitters in solution does not approach zero as it would in a single-molecule correlation experiment. Because there is a Poisson distribution of particles in the focal volume, there is a uniform probability at all τ of measuring photon pairs produced by different particles. This probability, given by the long τ limit of $g^{(2)}(\tau)$, is normalized to unity in the FCS correlation function. Thus, the antibunching feature of single-photon emitters in FCS decays to one instead of zero. In fact, antibunching features that approach a value above unity have been used elsewhere to identify aggregation in both organic dyes and NCs because aggregated particles will behave as multiphoton emitters.[30,31]

To extend the SM-$g^{(2)}$ formalism of Nair et al.[19] to a solution-phase measurement, we have modified FCS by using pulsed excitation instead of continuous-wave excitation (Figure 1a). This allows us to use photon correlation to study biexciton recombination dynamics at the ensemble level. In Figure 1b, we show an example of a typical raw histogram of correlation counts (i.e., the numerator of eq 1) measured using pulsed excitation and a solution-phase sample. As in a single-molecule $g^{(2)}(\tau)$, the solution-phase $g^{(2)}(\tau)$ is characterized by a series

of peaks at the repetition period of the excitation laser. However, here, the integrated areas of these peaks are modulated by the diffusion physics of the sample. The center peak at $\tau = 0$ exhibits an increased area compared to that measured by SM-$g^{(2)}$ due to the detection of photon pairs from different particles, and the integrated areas of the other correlation peaks decay on the time scale of particle diffusion. This point is emphasized in Figure 1c, which shows that when the normalized $g^{(2)}(\tau)$ is calculated by integrating over each correlation peak, it reproduces the FCS correlation function and can inform on both the average occupation of particles in the focal volume and their average dwell time.

As derived in the Supporting Information, the center-to-side peak ratio produced by a focal volume of fluorophores freely and independently diffusing in solution can be related to the average BX/X quantum yield ratio via

$$\frac{g_0^{(2)}}{g_{T_{\mathrm{rep}}}^{(2)}} = \frac{\langle n \rangle}{\langle n \rangle + 1} + \frac{1}{\langle n \rangle + 1} \frac{\langle \gamma_{\mathrm{x}} \gamma_{\mathrm{bx}} \rangle}{\langle \gamma_{\mathrm{x}}^2 \rangle} \quad (3)$$

where $\langle \cdots \rangle$ is still a time average over the integration time of the experiment, but now reports on the average properties of all particles that pass through the focal volume, and $\langle n \rangle$ represents the average occupancy of the focal volume as measured by FCS (or the peak-integrated $g^{(2)}(\tau)$ from Figure 1c). The right side of eq 3 illustrates the distinction between the two types of photon pairs that contribute to the signal of solution-phase experiments. The first term is derived from photon pairs from different particles, which are equally likely to be detected in the center and side peaks and do not contribute an antibunching signal. The second term is derived from photon pairs from the same particle, which are more likely to occur in the side peak than the center peak and contribute an antibunching signal according to eq 2. The average occupancy uniquely dictates the relative weights of these two signals.

Alternatively, as also shown in the Supporting Information, eq 3 can be rearranged to evoke the standard FCS formalism,

$$\frac{\langle \gamma_{\mathrm{x}} \gamma_{\mathrm{bx}} \rangle}{\langle \gamma_{\mathrm{x}}^2 \rangle} = \frac{g_0^{(2)} - 1}{g_{T_{\mathrm{rep}}}^{(2)} - 1} \quad (4)$$

This representation emphasizes that in FCS, the unity Poisson background is the interparticle contribution to $g^{(2)}(\tau)$, so it can simply be subtracted to isolate the single-particle contribution. A sample with no biexciton fluorescence will exhibit full antibunching to the unity baseline, as is observed for FCS measurements on organic dyes,[28] whereas a sample with equal biexciton and exciton quantum yields will not exhibit any antibunching.

To confirm these theoretical results, we use S-$g^{(2)}$ to measure a set of serial dilutions of a sample of CdSe/CdS core/shell NCs (see Supporting Information for synthetic details). The center-to-side peak area ratios of each dilution are shown as a function of the average occupation of the focal volume, as measured by an FCS fit of the peak-integrated $g^{(2)}(\tau)$ (Figure 2a). Trend lines are included to show the concentration-dependence predicted by eq 3 for several possible BX/X quantum yield ratios. In Figure 2b, we show the corresponding BX/X quantum yield ratios for each dilution according to eq 4, with error bars given by the

standard deviation of the shot noise of each measurement. This experiment confirms the predicted concentration dependence of the peak area ratio and highlights the remarkable consistency of our measurement.

Several key points are essential for the reliable interpretation of the S-$g^{(2)}$ experiment. First, both the SM-$g^{(2)}$ and S-$g^{(2)}$ experiments must be carried out under low flux excitation to use the simplified approximation of the Poisson distribution used to derive eqs 2–4. In the S-$g^{(2)}$ experiment, an average excitation rate of less than 0.1 excitations per pulse in the entire focal volume guarantees quantitative accuracy on the order of 1%. Second, because clusters of NCs are known to exhibit decreased antibunching,[31] sample aggregation can produce artificially high quantum yield ratios. The consistent quantum yield ratio measured upon serial dilution in Figure 2 indicates that our sample preparation minimizes additional aggregation, but suspicious samples may be analyzed by techniques such as photon counting histogram analysis to confirm that multiparticle aggregates are not biasing the measurement.[32,33] Finally, although the S-$g^{(2)}$ experiment measures the average BX/X quantum yield ratio of an entire sample without user selection bias, the intensity-weighted averages in this observable are intrinsically weighted toward bright emitters. When interpreting the sample-averaged BX/X quantum yield ratio of an entire sample, it must be noted that nonemissive particles or dark “blinking” states are not interrogated because they contribute to neither the center nor the side correlation peaks,[19] and the average BX quantum yield cannot be calculated by multiplying the BX/X quantum yield ratio and the overall sample X quantum yield.

We present two sets of measurements to highlight the utility and broad applicability of the S-$g^{(2)}$ technique. First, we demonstrate that it can be straightforwardly applied to study synthetically underdeveloped materials. One of the limitations of the SM-$g^{(2)}$ experiment is that it requires samples to be optimized for single-molecule spectroscopy. Studied emitters must have high quantum yields to provide a strong single-molecule fluorescence signal under low excitation flux, and they must have fluorescence stability on the order of tens of minutes to measure the quantum yield ratio with precision near 1%. These requirements are further exacerbated when measuring samples with long fluorescence lifetimes because longer laser repetition periods further reduce photon count rate. In contrast, S-$g^{(2)}$ measurements do not require fluorescence stability because of the rapid exchange of particles in the focal volume, and the duration of S-$g^{(2)}$ experiment can be extended arbitrarily to compensate for the weak fluorescence signals produced by samples with low quantum yields or long fluorescence lifetimes.

In Figure 3, we show peak-integrated solution-phase $g^{(2)}(\tau)$ for three types of NC samples that are not usually studied using single-NC spectroscopy: CdSe cores, which are normally overcoated for improved quantum yield and fluorescence stability; InP/ZnS core/shell NCs, which are a cadmium-free alternative to CdSe NCs; and visible-emitting InAs/ZnS NCs, which are also a promising infrared-emitting material.[4] The biexciton quantum yields of all three samples are very low. The measurement of our InAs/ZnS sample sets an upper bound on the quantum yield ratio of 0.8% percent, in agreement with transient absorption measurements reporting biexciton lifetimes under 100 ps.[34,35] This result is consistent with a very recent SM-$g^{(2)}$ investigation of larger, infrared-emitting InAs/CdZnS NCs, which

reported a wide distribution of quantum yield ratios with most particles exhibiting ratios below 5% and a few outliers exhibiting significantly larger values.[36] The biexciton/exciton quantum yield ratio of our sample was expected to be even lower than those reported by Bischof et al. due to the increased quantum confinement in our visible-emitting sample.[15] Our technique also reveals that, even with an epitaxial shell to enhance exciton fluorescence, current InP samples do not appear to offer a multiexciton advantage over CdSe cores. This finding is consistent with the very recent report from Mangum et al.,[37] which found BX/X quantum yield ratios less than 5% in type II InP/CdS core/shell NCs. Deliberate synthetic design with the BX quantum yield in mind will be required to optimize these NC samples for high-flux applications.

One synthetic parameter that has been used to demonstrate the potential for synthetic control over the BX quantum yield in CdSe NCs is the growth of a CdS shell. Quasi-type II heterostructures such as CdSe/CdS NCs generally have reduced Auger rates compared to core-only and type I heterostructures because of the reduced overlap between their electron and hole wave functions, but this decreased non-radiative recombination rate is also accompanied by a decreased radiative rate.[21,38] Nevertheless, recent syntheses of thick-shelled CdSe/CdS NCs using multiday SILAR procedures have been shown to have anomalously low Auger rates,[16,39] with BX/X quantum yield ratios approaching 40% in 19-monolayer samples.[20] Enhanced biexciton emission compared to that predicted by electron–hole overlap could be attributed to several possible factors, including a smoothing of the core/shell potential boundary via core/shell alloying,[16,40] by a reduction in local electric fields via trap passivation,[41] or by the elimination of trap-mediated Auger pathways.[42,43] Recently, Klimov and co-workers[21,44] introduced a rapid shell growth procedure designed to eliminate unintentional core/shell alloying to identify the possible role of the potential boundary in multiexciton recombination. They found that their rapid shell growth resulted in extremely low BX quantum yields unless they attempted to introduced an alloy region by dual precursor injection. Although this finding conclusively demonstrates the importance of the core/shell interface in controlling BX fluorescence, it is still unclear whether the only difference between their intentionally alloyed and reference samples is a smoother potential boundary. The other proposed sources of Auger enhancement relating to surface trapping may also be affected by their alloying procedure, especially given that their X quantum yields can dip below 50%.[21]

Our group recently presented a different rapid CdS shell growth procedure that also uses relatively nonreactive precursors and high reaction temperatures.[22] These reaction conditions should result in NCs with similar interfacial alloying as the reference samples measured by Park et al.,[21] which were not intentionally alloyed. However, NCs produced by our synthesis have higher X quantum yields, exceeding 85% for shells as thick as 5.0 nm (14 monolayers). In Figure 4, we use the S-$g^{(2)}$ technique to investigate the multiexciton recombination dynamics of a shell series of particles made by our optimized synthesis. Their BX/X quantum yield ratios, which roughly approximate the actual BX quantum yields due to their high X quantum yields, increase monotonically with shell growth in a fashion consistent with the multiday SILAR shell growth.[20] These results show that intentional alloying is not required to increase the BX quantum yield of CdSe NCs using a rapid CdS

shell growth. Unless rapid shell growths are capable of producing the considerable core/shell alloying that has been hypothesized to occur in multiday SILAR procedures, other sources of Auger enhancement must play an active role in defining the BX quantum yield of CdSe/CdS core/shell samples. Furthermore, we note that the BX/X quantum yield ratio in our shell growth has not yet reached a plateau with increased shell thickness; further increases in the BX/X quantum yield ratio should be possible by extending our synthesis to even thicker shells. The S-$g^{(2)}$ technique is an ideal tool for further optimizing multiexcitonic properties and for investigating the interfacial physics behind these synthetic discrepancies in the BX/X quantum yield ratio.

In conclusion, we have demonstrated a solution-phase photon correlation measurement capable of measuring the average biexciton/exciton quantum yield ratio of an entire sample without user selection bias. This technique can be used to investigate a wide scope of samples not neccessarily optimized for standard single-molecule spectroscopy, and provides a reliable single-molecule alternative to ultrafast techniques for investigating multiexciton recombination dynamics at the ensemble level. We have applied this method to measure notably weak biexciton fluorescence in NC samples of visible-emitting InP/ZnS and InAs/ZnS and to demonstrate increased biexciton fluorescence in our recent rapid CdSe/CdS shell growth. Furthermore, it should be straightforward to adapt solution-phase antibunching measurements for characterizing developing infrared-emitting nanomaterials using recent innovations in short-wave infrared single-photon detection.[45]

Experimental Methods

Optical Setup and Analysis

Solution-phase samples were excited by a 532 nm pulsed laser (Picoquant, Repetition rate between 2.5 and 0.5 MHz, ≈50 ps pulse width) via a home-built confocal epifluorescence microscope constructed using a 10:90 R/T visible non-polarizing beamsplitter (Thorlabs, BS025) and an infinity-corrected water-immersion objective (Nikon, Plan Apo VC 60× WI, NA 1.2). Emission from the focal volume was recollimated, spatially filtered using a pinhole (10 cm focal length focusing lens, 50 μm pinhole, and 5 cm focal length recollimating lens), and spectrally filtered using a 532/10 nm notch filter (Chroma, ZET532/10×) to remove laser scatter. Then, the emission was split using a 50:50 nonpolarizing beamsplitter (Newport, 20BC17MB.1), spectrally filtered using either 700 or 800 nm short-pass filters (Thorlabs, FESH0700 and FES0800), and focused onto two single-photon-counting APDs (Excelitas, SPCM-AQRH-16). The detected photon arrivals were recorded in memory along with the sync signal from the laser using a Picoquant Hydraharp operating in time-tagged-time-resolved mode and correlated in postprocessing using custom software (see Supporting Information of Bischof et al.[36]). Integration times varied from 1 to 4 h, depending on the laser repetition rate and the quantum yield of the sample. Pulse-integrated correlation functions were calculated according to the procedure described by Bischof et al.[36] and fit using the single-species 2D diffusion model to recover the average occupancy used in eq 3.[27] The $\tau \rightarrow 0$ limit of this FCS fit was also used as $g^{(2)}_{T_{rep}}$ in eq 4 to correct for any particle diffusion that occurred on the time scale of the repetition rate of the laser (see Supporting Information).

Sample Preparation

Dilute solution-phase NC samples were created by adding between 0.5 and 20 μL of visibly colored, concentrated NC/hexane solution to a solution composed of 0.5 mL of hexanes and several drops of a solution of 1.25 mL of 0.2 M cadmium oleate, 100 μL of *n*-decylamine, and 8.75 mL of toluene, to produce an average occupation in the focal volume between 1 and 3 (unless otherwise specified). This solution was wicked into a rectangular capillary (VitroCom, 0.10 × 2.00 mm i.d.) and sealed with capillary tube sealant to prevent evaporation. A freshly diluted sample was made for each measurement to avoid aggregation except for in the serial dilution experiment.

Supplementary Material

Refer to Web version on PubMed Central for supplementary material.

ACKNOWLEDGMENTS

This work was primarily supported by the U.S. Department of Energy (DOE), Office of Science, Basic Energy Sciences (BES), under Award No. DE-FG02-07ER46454. T.S.B. acknowledges partial support from the excitonic EFRC at MIT, an Energy Frontier Research Center funded by the U.S. Department of Energy (DOE), Office of Science, Basic Energy Sciences (BES), under Award No. DE-SC0001088. I.C. acknowledges support from the National Science Foundation Graduate Research Fellowship Program. D.K.H. acknowledges support from the National Institutes of Health funded Laser Biomedical Research Center at MIT under Award No. 9P41EB015871-26A1 (Synthesis of InAs-based nanocrystals).

REFERENCES

1. Tsien, RY.; Ernst, L.; Waggoner, A. Handbook of Biological Confocal Microscopy. Pawley, JB., editor. New York: Springer; 2006. p. 338-352.
2. Chen O, Zhao J, Chauhan VP, Cui J, Wong C, Harris DK, Wei H, Han H-S, Fukumura D, Jain RK, Bawendi MG. Nat. Mater. 2013; 12:445–451. [PubMed: 23377294]
3. Boldt K, Kirkwood N, Beane GA, Mulvaney P. Chem. Mater. 2013; 25:4731–4738.
4. Chen O, Wei H, Maurice A, Bawendi MG, Reiss P. MRS Bull. 2013; 38:696–702.
5. Talapin DV, Lee J-S, Kovalenko MV, Shevchenko EV. Chem. Rev. 2010; 110:389–458. [PubMed: 19958036]
6. Lhuillier E, Keuleyan S, Liu H, Guyot-Sionnest P. Chem. Mater. 2013; 25:1272–1282.
7. Lhuillier E, Keuleyan S, Zolotavin P, Guyot-Sionnest P. Adv. Mater. 2013; 25:137–141. [PubMed: 23027629]
8. Harris DK, Allen PM, Han H-S, Walker BJ, Lee J, Bawendi MG. J. Am. Chem. Soc. 2011; 133:4676–4679. [PubMed: 21388210]
9. Fisher BR, Eisler H-J, Stott NE, Bawendi MG. J. Phys. Chem. B. 2004; 108:143–148.
10. Wehrenberg BL, Wang C, Guyot-Sionnest P. J. Phys. Chem. B. 2002; 106:10634–10640.
11. Warner JH, Thomsen E, Watt AR, Heckenberg NR, Rubinsztein-Dunlop H. Nanotechnology. 2005; 16:175–179. [PubMed: 21727420]
12. Klimov VI. Annu. Rev. Phys. Chem. 2007; 58:635–673. [PubMed: 17163837]
13. Pandey A, Guyot-Sionnest P. J. Chem. Phys. 2007; 127:111104. [PubMed: 17887819]
14. Zhao J, Chen O, Strasfeld DB, Bawendi MG. Nano Lett. 2012; 12:4477–4483. [PubMed: 22871126]
15. Klimov VI, Mikhailovsky AA, McBranch DW, Leatherdale CA, Bawendi MG. Science. 2000; 287:1011–1013. [PubMed: 10669406]
16. García-Santamaría F, Brovelli S, Viswanatha R, Hollingsworth JA, Htoon H, Crooker SA, Klimov VI. Nano Lett. 2011; 11:687–693. [PubMed: 21207930]

17. Qin W, Liu H, Guyot-Sionnest P. ACS Nano. 2014; 8:283–291. [PubMed: 24350673]
18. Tyagi P, Kambhampati P. J. Chem. Phys. 2011; 134:094706. [PubMed: 21384996]
19. Nair GP, Zhao J, Bawendi MG. Nano Lett. 2011; 11:1136–1140. [PubMed: 21288042]
20. Park Y-S, Malko AV, Vela J, Chen Y, Ghosh Y, García-Santamaría F, Hollingsworth JA, Klimov VI, Htoon H. Phys. Rev. Lett. 2011; 106:187401. [PubMed: 21635124]
21. Park Y-S, Bae WK, Padilha LA, Pietryga JM, Klimov VI. Nano Lett. 2014; 14:396–402. [PubMed: 24397307]
22. Coropceanu I, Bawendi MG. Nano Lett. 2014; 14:4097–4101. [PubMed: 24902615]
23. Cui J, Beyler AP, Bischof TS, Wilson MWB, Bawendi MG. Chem. Soc. Rev. 2014; 43:1287–1310. [PubMed: 24280771]
24. Hanbury Brown R, Twiss RQ. Nature (London UK). 1956; 177:27–29.
25. Lounis B, Moerner WE. Nature. 2000; 407:491–493. [PubMed: 11028995]
26. Brokmann X, Giacobino E, Dahan M, Hermier JP. Appl. Phys. Lett. 2004; 85:712.
27. Webb, WW. Fluorescence Correlation Spectroscopy: Theory and Applications. Rigler, R.; Elson, EL., editors. Berlin: Springer; 2001. p. 305-330.
28. Mets, U. Fluorescence Correlation Spectroscopy: Theory and Applications. Rigler, R.; Elson, EL., editors. Berlin: Springer; 2001. p. 346-359.
29. Larson DR, Zipfel WR, Williams RM, Clark SW, Bruchez MP, Wise FW, Webb WW. Science. 2003; 300:1434–1436. [PubMed: 12775841]
30. Sýora J, Kaiser K, Gregor I, Bönigk W, Schmalzing G, Enderlein J. Anal. Chem. 2007; 79:4040–4049. [PubMed: 17487973]
31. Bussian DA, Malko AV, Htoon H, Chen Y, Hollingsworth JA, Klimov VI. J. Phys. Chem. C. 2009; 113:2241–2246.
32. Chen Y, Müller JD, So PT, Gratton E. Biophys. J. 1999; 77:553–567. [PubMed: 10388780]
33. Huang B, Perroud TD, Zare RN. ChemPhysChem. 2004; 5:1523–1531. [PubMed: 15535551]
34. Ben-Lulu M, Mocatta D, Bonn M, Banin U, Ruhman S. Nano Lett. 2008; 8:1207–1211. [PubMed: 18341299]
35. Schaller RD, Pietryga JM, Klimov VI. Nano Lett. 2007; 7:3469–3476. [PubMed: 17967043]
36. Bischof TS, Correa RE, Rosenberg D, Dauler EA, Bawendi MG. Nano Lett. 2014
37. Mangum BD, Wang F, Dennis AM, Gao Y, Ma X, Hollingsworth JA, Htoon H. Small. 2014; 10:2892–2901. [PubMed: 24715631]
38. Brovelli S, Schaller RD, Crooker SA, García-Santamaría F, Chen Y, Viswanatha R, Hollingsworth JA, Htoon H, Klimov VI. Nat. Commun. 2011; 2:280. [PubMed: 21505436]
39. Chen Y, Vela J, Htoon H, Casson JL, Werder DJ, Bussian DA, Klimov VI, Hollingsworth JA. J. Am. Chem. Soc. 2008; 130:5026–5027. [PubMed: 18355011]
40. Cragg GE, Efros AlL. Nano Lett. 2010; 10:313–317. [PubMed: 20017564]
41. Jiang Z-J, Kelley DF. Nano Lett. 2011; 11:4067–4073. [PubMed: 21916485]
42. Mangum BD, Sampat S, Ghosh Y, Hollingsworth JA, Htoon H, Malko AV. Nanoscale. 2014; 6:3712–3720. [PubMed: 24569861]
43. Cohn AW, Schimpf AM, Gunthardt CE, Gamelin DR. Nano Lett. 2013; 13:1810–1815. [PubMed: 23464673]
44. Bae WK, Padilha LA, Park Y-S, McDaniel H, Robel I, Pietryga JM, Klimov VI. ACS Nano. 2013; 7:3411–3419. [PubMed: 23521208]
45. Correa RE, Dauler EA, Nair G, Pan SH, Rosenberg D, Kerman AJ, Molnar RJ, Hu X, Marsili F, Anant V, Berggren KK, Bawendi MG. Nano Lett. 2012; 12:2953–2958. [PubMed: 22624846]

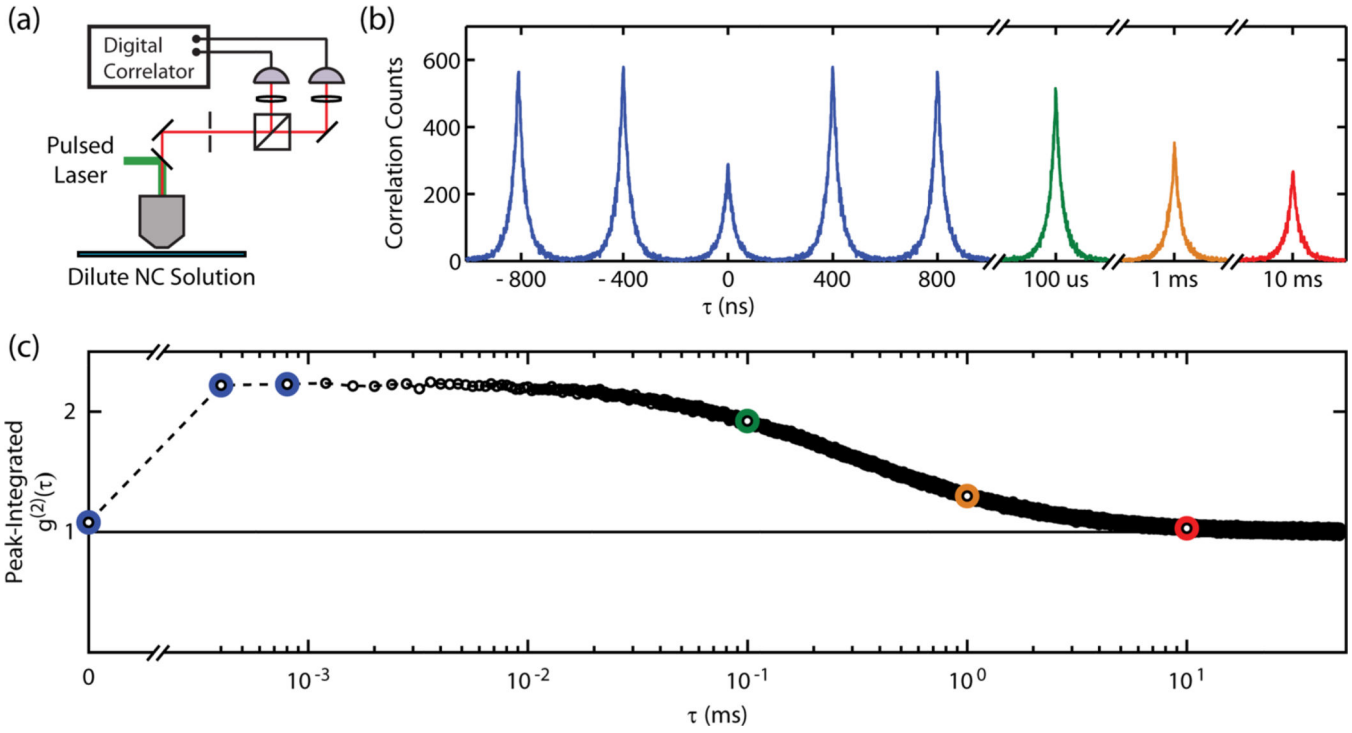

Figure 1.

(a) The S-$g^{(2)}$ experimental apparatus uses a pulsed laser to excite a solution-phase sample. (b) An example of a histogram collected during an S-$g^{(2)}$ measurement of detected photon pairs as a function of their temporal separation τ. The "center peak" at τ = 0 represents the number of photon pairs originating from the same excitation pulse, whereas the "side peaks" at integer multiples of the laser repetition period represent the number of photon pairs originating from different excitation pulses. (c) The peak-integrated intensity correlation function is created by normalizing the area of the correlation peaks in (b) according to eq 1. A center peak area above unity is indicative of BX fluorescence and the side peak areas sample the FCS correlation function.

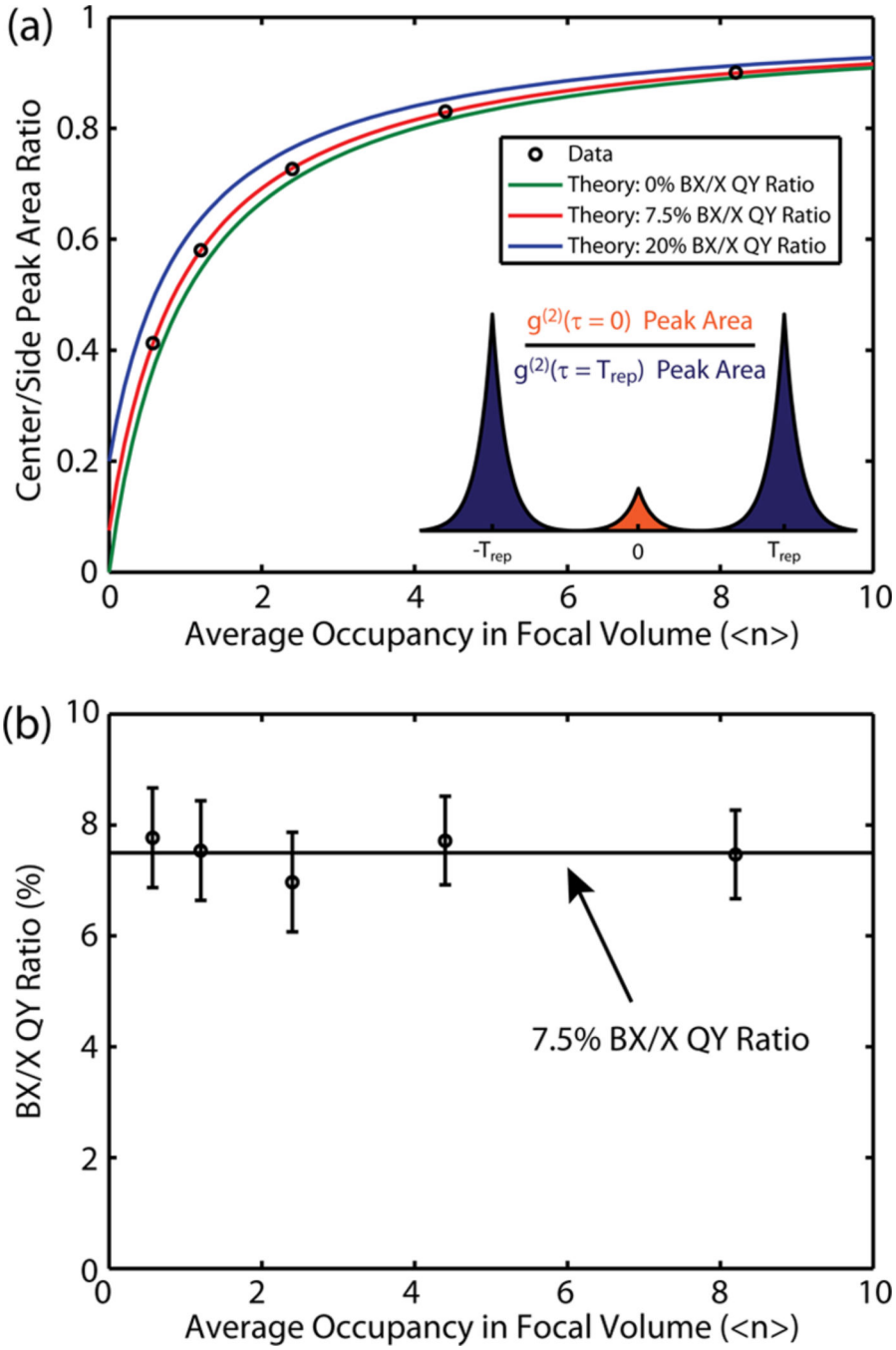

Figure 2.

(a) The center-to-side peak area ratio of a CdSe/CdS sample upon serial dilution, with trend lines given by eq 3. (b) Corresponding BX/X quantum yield ratios as calculated from eq 4 with error bars given by the standard deviation of shot noise. Serial dilution does not cause any systematic changes in the measured quantum yield ratio and both representations are consistent with a BX/X quantum yield ratio of 7.5%.

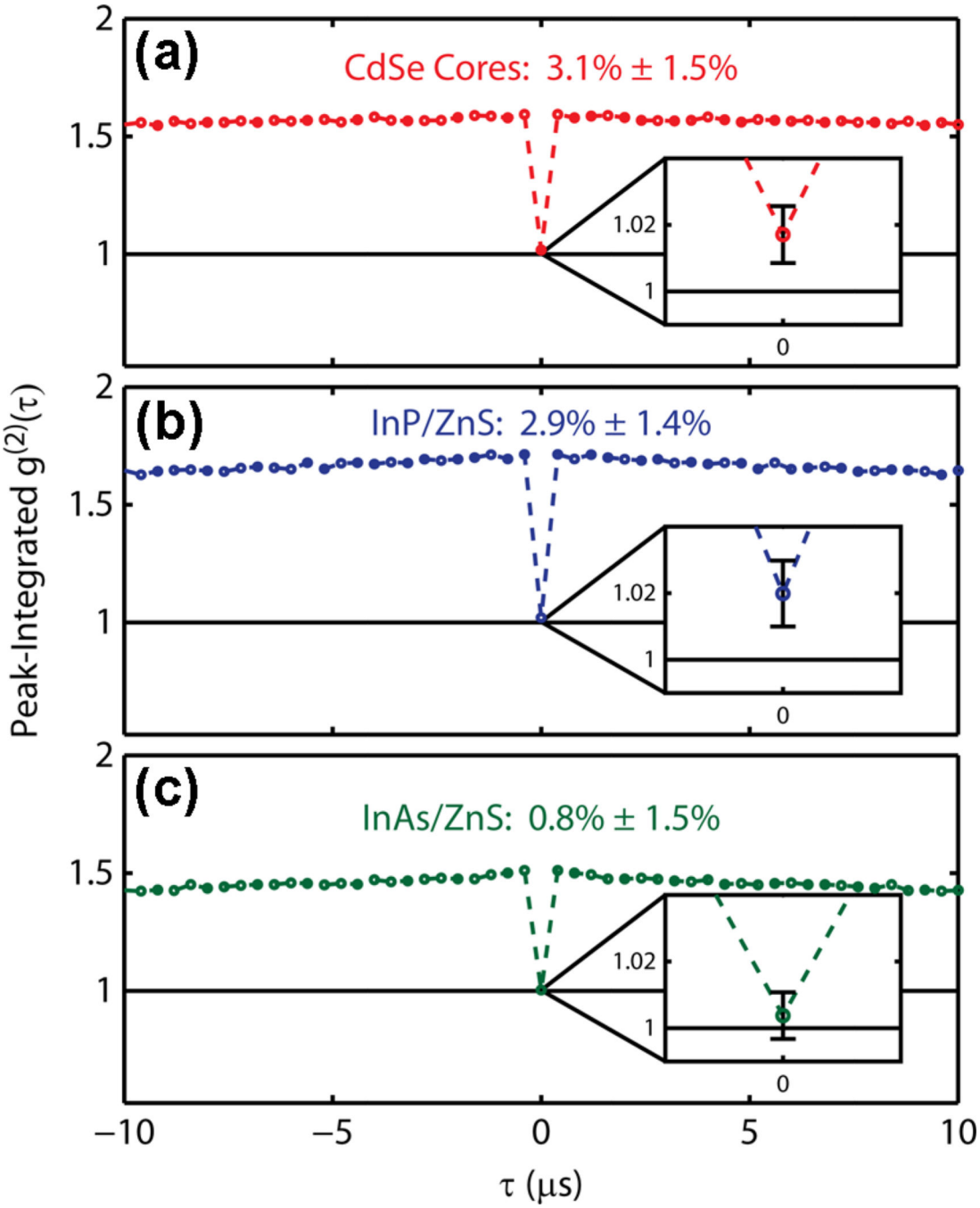

Figure 3.

Peak-integrated $g^{(2)}(\tau)$ measured by S-$g^{(2)}$ for samples of (a) CdSe cores, (b) visible-emitting InP/ZnS core/shell NCs, and (c) visible-emitting InAs/ZnS core/shell NCs. Corresponding BX/X quantum yield ratios are noted and the insets magnify their respective center-peak value. Reported uncertainties and center-peak error bars are given by the standard deviation of shot noise. All three samples exhibit very little BX emission, with antibunching features approaching the interparticle Poisson background.

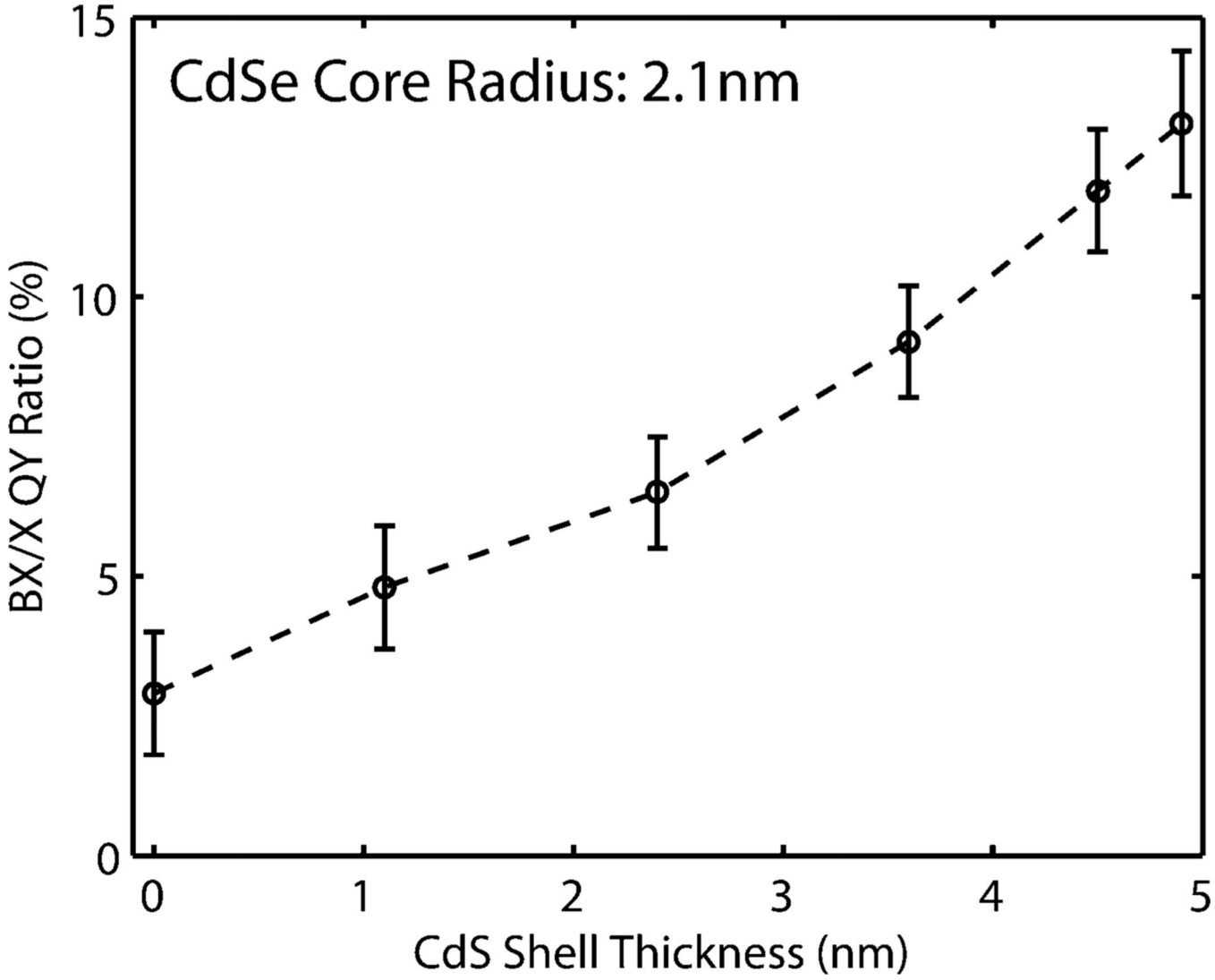

Figure 4.

BX/X quantum yield ratios of a shell-thickness series of CdSe/CdS core/shell NCs synthesized using the rapid shell growth developed by Coropceanu et al.[22] The quantum yield ratio rises monotonically with increasing shell thickness during this rapid synthetic procedure as it does for NCs produced with multiday SILAR procedures.